

Design of the Advanced Light Source elliptical wiggler

Chun-Xi Wang *, Ross Schlueter, Egon Hoyer, Phil Heimann

Advanced Light Source, Lawrence Berkeley Laboratory, University of California, Berkeley, CA 94720, USA

The elliptical wiggler is a circularly polarized light source capable of providing very broad spectral coverage and a high degree of circular polarization. The main features of an elliptical wiggler can be understood through analogy to bending magnet radiation. However, some aspects, such as the end structure's influence on the degree of circular polarization, require more elaborate methods to characterize. We present an algorithm based on the stationary-phase method, which allows calculation of radiation properties from an arbitrary electron trajectory, so a non-sinusoidal magnetic field's influence on the radiation performance can be taken into account. We show general radiation properties of an elliptical wiggler and discuss factors affecting the radiation produced. Practical issues encountered during the conceptual design of an elliptical wiggler at the Advanced Light Source are addressed.

1. Introduction

An elliptical wiggler was first proposed and built in Japan [1]. As with other types of wigglers, radiation from an elliptical wiggler can be viewed as coming from a series of small bending magnets (dipoles). For a bending magnet source, radiation is elliptically polarized off the midplane. The handedness of polarization depends on the magnetic field direction and the sign of the vertical observation angle. In a planar wiggler the off-midplane radiation tends to be unpolarized instead of elliptically-polarized due to the mixing of different handedness photons from successive dipoles. In an elliptical wiggler, a horizontal magnetic field is superimposed on the primary vertical field, alternately tilting up, then down, the series of dipole sources. Off-axis radiation from each dipole is observed on the nominal beam axis, such that, for successive dipoles, both the vertical magnetic field direction and relative observation angle change signs, so the photon handedness does not change. Thus, highly circularly-polarized light can be generated on the beam axis in an elliptical wiggler. The main radiation features of an elliptical wiggler result from the superposition of two sets of dipole sources, one tilting upward and the other downward. A complete evaluation of the performance of an elliptical wiggler needs to take into account practical factors such as non-ideal magnetic field and end pole influence. In section 2, based on the stationary-phase method, we develop a versatile algorithm capable of calculating the radiation from wigglers of any magnetic field structure. This algorithm has been integrated in the radiation calculation software RADID [2], and is complementary to the algorithm for undulators

based on the FFT method [3]. In section 3, we present a panoramic view of the spectral and angular distributions of the flux and polarization degree of an elliptical wiggler. In section 4, we report some practical considerations in the conceptual design of the Advanced Light Source (ALS) elliptical wiggler.

2. Stationary-phase method

The spectral angular distribution of the radiation generated by a moving electron ($R \gg \gamma\lambda$) is given by [4]:

$$\frac{d^2I}{d\omega dA} = \frac{\alpha\hbar}{4\pi^2} \left| \frac{\mathbf{n} \times \mathbf{n} \times \boldsymbol{\beta}}{(1 - \mathbf{n} \cdot \boldsymbol{\beta})R} e^{i\omega(\tau + \frac{R(\tau)}{c})} \right|_{\Gamma} - i\omega \int_{\Gamma} \frac{1}{R} \mathbf{n} \times \mathbf{n} \times \boldsymbol{\beta} e^{i\omega(\tau + \frac{R(\tau)}{c})} d\tau \Big|^2, \quad (1)$$

where the domain Γ can be any interval including the accelerating region. The boundary term can be significant at very low energy, say in the far-infrared, but is negligible when the energy is high enough to guarantee applicability of the stationary phase method [2,5]. When the exponential phase term oscillates so rapidly that most parts of the integrand cancel each other, the contribution to the integral comes from the neighborhood of the stationary phase or saddle points, where the phase changing is the slowest. Thus, we can expand the phase at these points and integrate with the approximate phase functions, which are good in the neighborhood of the expansion points. Based on this method, we have developed a successful radiation calculation algorithm for general 1D magnetic device in ref. [2]. Here we update it into a versatile 3D algorithm, employing a new calculation method for phase expansion coefficients.

* Corresponding author. Present address: Applied Physics Department Stanford University, Stanford, CA 94305-4090, USA.

The phase is determined by the observer time $t = \tau + R(\tau)/c$. Expanding it into a Taylor series we have

$$t = \sum_{n=0}^{\infty} \frac{t^{(n)}(\tau_s)}{n!} (\tau - \tau_s)^n, \quad (2)$$

where $t^{(0)} = \tau_s + R(\tau_s)/c \equiv t_s$, $t^{(1)} = 1 - \mathbf{n} \cdot \boldsymbol{\beta}$, $t^{(2)} = -(\mathbf{n} \cdot \boldsymbol{\beta})' = 0$, $t^{(3)} = -(\mathbf{n} \cdot \boldsymbol{\beta})''$, and so on. The $t^{(0)}$ determines the interferences among the radiation from different parts of a trajectory. The $t^{(1)}$ determines the phase changing rate. The requirement of slowest changing rate implies $t^{(2)} = 0$, so this is the condition that locates the stationary phase points. This condition is consistent with the well-known fact that radiation comes mainly from the tangent direction of a trajectory. As before, we keep only up to the third-order term. To evaluate the detailed phase expansion, we assume only magnetic field is present and the electron's equation of motion is:

$$\dot{\boldsymbol{\beta}} = \kappa \boldsymbol{\beta} \times \mathbf{B}, \quad \text{where } \kappa = -\frac{e}{\gamma m}. \quad (3)$$

The derivatives of $\mathbf{n} \cdot \boldsymbol{\beta}$ are calculated via:

$$\begin{aligned} \dot{\mathbf{n}} &= \frac{c}{R} \mathbf{n} \times (\mathbf{n} \times \boldsymbol{\beta}) = \frac{c}{R} (\mathbf{n} \cdot \boldsymbol{\beta} \mathbf{n} - \boldsymbol{\beta}), \\ \ddot{\mathbf{n}} &= \frac{c}{R} [(\mathbf{n} \cdot \boldsymbol{\beta})' \mathbf{n} + 2(\mathbf{n} \cdot \boldsymbol{\beta}) \dot{\mathbf{n}} - \dot{\boldsymbol{\beta}}], \end{aligned} \quad (4)$$

$$\ddot{\mathbf{n}} \cdot \boldsymbol{\beta} + 2\dot{\mathbf{n}} \cdot \dot{\boldsymbol{\beta}} = 3\frac{c}{R} \mathbf{n} \cdot \boldsymbol{\beta} (\mathbf{n} \cdot \boldsymbol{\beta})' - 3\frac{c}{R} \boldsymbol{\beta} \cdot \dot{\boldsymbol{\beta}} = 0.$$

The last identity is due to the stationary-phase requirement and the energy conservation of electrons in a pure magnetic field. So we have:

$$\begin{aligned} (\mathbf{n} \cdot \boldsymbol{\beta})'' &= \ddot{\mathbf{n}} \cdot \boldsymbol{\beta} + 2\dot{\mathbf{n}} \cdot \dot{\boldsymbol{\beta}} + \mathbf{n} \cdot \ddot{\boldsymbol{\beta}} = \mathbf{n} \cdot (\kappa \boldsymbol{\beta} \times \mathbf{B})' \\ &= -\kappa^2 B^2 \mathbf{n} \cdot \boldsymbol{\beta} + \kappa^2 \mathbf{n} \cdot \mathbf{B} \boldsymbol{\beta} \cdot \mathbf{B} + \kappa (\mathbf{n} \times \boldsymbol{\beta}) \cdot \dot{\boldsymbol{\beta}}. \end{aligned} \quad (5)$$

Compared to the first term, the second term can be dropped because usually \mathbf{n} and $\boldsymbol{\beta}$ are roughly parallel, and are perpendicular to the magnetic field \mathbf{B} . The ratio of the last term to the first is

$$\sim \omega_B^{-1} (\mathbf{n} \times \boldsymbol{\beta}) \cdot \dot{\boldsymbol{\beta}} / B \sim \frac{m_e c}{e} \frac{dB}{dz} / B^2 \sim 10^{-3} \frac{dB}{dz} / B^2,$$

which for usual B is $\ll 1$. Therefore the phase can be expanded as:

$$\begin{aligned} \omega t &= \omega t_s + \omega(1 - \mathbf{n} \cdot \boldsymbol{\beta})(\tau - \tau_s) \\ &\quad + \omega \frac{1}{6} \kappa^2 B^2 \mathbf{n} \cdot \boldsymbol{\beta} (\tau - \tau_s)^3 + \dots \\ &\equiv \omega t_s + \frac{3}{2} \zeta \left(\xi + \frac{1}{3} \xi^3 \right) + \dots, \end{aligned} \quad (6)$$

where

$$\begin{aligned} \xi &= \frac{1}{\sqrt{2}} \kappa |\mathbf{B}| \sqrt{\frac{\mathbf{n} \cdot \boldsymbol{\beta}}{1 - \mathbf{n} \cdot \boldsymbol{\beta}}} (\tau - \tau_s) \\ &\approx \frac{1}{\sqrt{2}} \kappa |\mathbf{B}| \frac{1}{\sqrt{1 - \mathbf{n} \cdot \boldsymbol{\beta}}} (\tau - \tau_s), \\ \zeta &= \frac{2\sqrt{2}}{3} \frac{\omega}{\kappa |\mathbf{B}|} \sqrt{\frac{(1 - \mathbf{n} \cdot \boldsymbol{\beta})^3}{\mathbf{n} \cdot \boldsymbol{\beta}}} \\ &\approx \frac{2\sqrt{2}}{3} \frac{\omega}{\kappa |\mathbf{B}|} (1 - \mathbf{n} \cdot \boldsymbol{\beta})^{3/2}. \end{aligned}$$

Next, we expand the vector part of the integrand of Eq. (1) at the stationary points. This part changes much slower than the phase term, so we keep the zero and first order terms. Noticing that the vector part is just $\dot{\mathbf{n}}/c$, we can get its expansion easily via Eq. (4):

$$\begin{aligned} \frac{\mathbf{n} \times (\mathbf{n} \times \boldsymbol{\beta})}{R} \\ = \frac{\dot{\mathbf{n}}}{c} \Big|_s + \left\{ \frac{1}{R} [2(\mathbf{n} \cdot \boldsymbol{\beta}) \dot{\mathbf{n}} - \dot{\boldsymbol{\beta}}] \right\}_s (\tau - \tau_s) + \dots \end{aligned} \quad (7)$$

Since

$$\frac{c}{R} (\mathbf{n} \cdot \boldsymbol{\beta})(\tau - \tau_s) \leq \frac{c(\tau - \tau_s)}{R} \ll 1,$$

the first term in the bracket is negligible compared to the zero order term. Using Eqs. (3) and (4):

$$\begin{aligned} \frac{\mathbf{n} \times (\mathbf{n} \times \boldsymbol{\beta})}{R} \\ = \left[\frac{1}{R} (\mathbf{n} \cdot \boldsymbol{\beta} \mathbf{n} - \boldsymbol{\beta}) \right]_s - \left[\frac{\kappa}{R} \boldsymbol{\beta} \times \mathbf{B} \right]_s (\tau - \tau_s) + \dots \\ \approx \left[\frac{1}{R} (\mathbf{n} - \boldsymbol{\beta}) \right]_s - \left[\frac{\kappa}{R} \boldsymbol{\beta} \times \mathbf{B} \right]_s (\tau - \tau_s) + \dots \end{aligned} \quad (8)$$

The expansion in both Eqs. (6) and (8) is up to the second derivative of \mathbf{n} . Higher order derivatives involve the magnetic field gradient. Combining Eqs. (6), (8) and (1), the flux density distribution is:

$$\begin{aligned} \frac{dF}{dA} &= \frac{\alpha}{3\pi^2} \frac{I \Delta \omega}{e} \left(\frac{\gamma m}{e} \omega \right)^2 \\ &\quad \times \left\{ \left| \sum_s e^{i\omega t_s} \left[\frac{1}{R} (\mathbf{n} - \boldsymbol{\beta}) \right]_s K_{1/3}(\xi_s) \right|^2 \right. \\ &\quad \left. + \left| \sum_s e^{i\omega t_s} \left[\frac{1}{R} \boldsymbol{\beta} \times \mathbf{B} \right]_s K_{2/3}(\xi_s) \right|^2 \right\}, \end{aligned} \quad (9)$$

where the summation is over all stationary points, $K_{1/3}$, $K_{2/3}$ are the well known modified Bessel functions and

$$s = \frac{\sqrt{2}}{|B|} \sqrt{\frac{1 - \mathbf{n} \cdot \boldsymbol{\beta}}{\mathbf{n} \cdot \boldsymbol{\beta}}} \approx \frac{\sqrt{2}}{|B|} \sqrt{1 - \mathbf{n} \cdot \boldsymbol{\beta}}.$$

Eq. (9) is a generalization of Eq. (19) in ref. [2]. This updated formula is a quite general result, applicable to arbitrary 3D magnetic field \mathbf{B} . Eq. (9) is the basis of the bending magnet approximation mentioned in the Introduction. Many results such as the bending magnet formula and the “dipole series model” can be deduced from Eq. (9). For wigglers, the summation can be moved out of the absolute square because of the incoherent superposition of radiation from different parts of a trajectory. Although further approximation of Eq. (9) is possible, it is simple enough for numerical calculations. Finding the stationary points and relevant values at those points is crucial for use of Eq. (9). For an arbitrary trajectory, there is no simple analytical method to find these stationary points according to the condition $(\mathbf{n} \cdot \boldsymbol{\beta}) = 0$. Numerically, we simply calculate $\mathbf{n} \cdot \boldsymbol{\beta}$ as a function of z and find its minimum values and corresponding positions numerically. The algorithm based on Eq. (9) has been integrated into the radiation calculation software RADID, by which we calculate the results shown below.

The polarization properties of the radiation are calculated via the coherency matrix and Stokes parameters that can be expressed in terms of the electric field components as follows [6]:

$$\mathbf{J} = \begin{pmatrix} J_{xx} & J_{xy} \\ J_{yx} & J_{yy} \end{pmatrix} = \begin{pmatrix} \langle E_x E_x^* \rangle & \langle E_x E_y^* \rangle \\ \langle E_y E_x^* \rangle & \langle E_y E_y^* \rangle \end{pmatrix} \quad \text{and} \quad (10)$$

$$\begin{aligned} S_0 &= J_{xx} + J_{yy} \\ S_1 &= J_{xx} - J_{yy} \\ S_2 &= J_{xy} + J_{yx} \\ S_3 &= -i(J_{xy} - J_{yx}), \end{aligned}$$

where $\langle \rangle$ represents the average over an ensemble of electrons. S_0 is normalized to the total flux density. The degree of circular polarization is: $P_c \equiv S_3/S_0$. Other properties can be calculated similarly.

3. Radiation properties of an elliptical wiggler

To satisfy user requirements for circularly polarized light, an elliptical wiggler has been proposed at the ALS, featuring 14 periods, $\lambda_w = 20$ cm, $B_y^{\max} = 2.0$ T, and $K_x^{\max} = 1.5$. The vertical and horizontal fields are produced by a permanent magnet/iron hybrid (PM) structure and an iron-core electromagnet (EM) structure, respectively [7]. Figs. 1a, b show the ideal sinusoidal fields (especially the end structure that will be discussed in detail later), velocities, and trajectories associated with the verti-

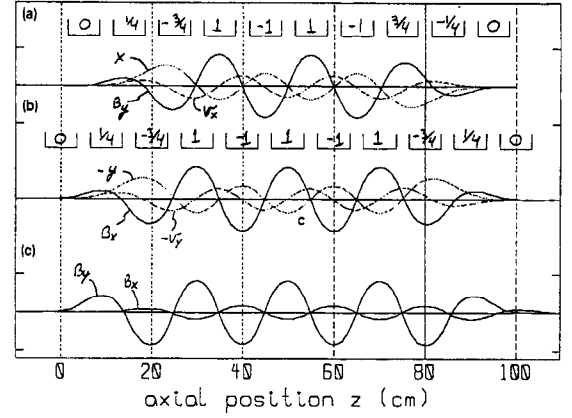


Fig. 1. (a) Vertical and (b) horizontal components of the magnetic field, velocity, and trajectory along the wiggler axis, showing the ends with the periodic section shortened. (c) Vertical and horizontal field components of earlier design with ends that have a deleterious effect on polarization. Marks above curves show pole tip positions and corresponding scalar potentials.

cal and horizontal structure, respectively. The horizontal field is shifted $\frac{1}{4}$ period from the vertical field to generate the elliptical trajectory. This phase shift results in maximum tilt of the dipoles with respect to the midplane when the vertical field is at its maximum.

In this section we provide a panoramic view of the radiation distribution of an elliptical wiggler. Ideal sinusoidal fields are used with $B_y = 2$ T, $K_x = 1.0$ and ALS storage ring parameters $E_e = 1.5$ GeV, $I = 400$ mA. Here we emphasize the general radiation features rather than exact values.

Flux density (photons/s/0.1%bw/mrad²/0.4 A) as a function of photon energy and vertical observation angle is shown in Fig. 2. The horizontal observation angle is zero. The two shoulders in the flux density plot correspond to the linearly-polarized “on-axis” radiation of the two sets of dipoles. The angle between the two shoulders is $2K_x/\gamma$. Polarization handedness changes when crossing these shoulders. Fig. 2 clearly illustrates the description of the radiation mechanism in the Introduction. As the photon energy decreases, the vertical angular distribution from each dipole increases, so the two shoulders gradually merge into one central peak. Circular polarization degree is high on-axis, and then changes sign, passing through zero at the two flux density shoulders. Polarization degree changes slowly at high photon energies and then drops sharply at energies below ~ 100 eV. Importantly, at high energies, the circular polarization peak is located in the valley of the flux density distribution. Decreasing K_x can bring the two shoulders closer and results in a higher on-axis flux density, but the degree of circular polarization drops. Thus there is a basic trade-off between the flux and degree of circular polarization.

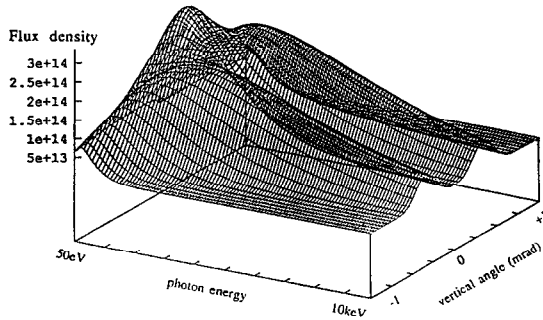


Fig. 2. Photon energy and vertical angle dependence of flux density.

Fig. 3 shows the distributions of circular polarization degree as a function of photon energy and horizontal observation angle. The vertical observation angle is zero. Horizontal flux distribution is rather flat over a wide range. Maximum horizontal fan width is $2K_y/\gamma$. Unlike the vertical angular flux distribution, the horizontal angular flux distribution does not change very much for different photon energies. Circular polarization degree is quite flat over the horizontal fan. The significant asymmetry in the angular distribution at high energy seen in Fig. 3 is due to the end field. To show the possible impact of the end structure, here we use a common end configuration (Fig. 1c), which includes a half peak pole at each end and has the strong vertical magnetic field spatially preceding the horizontal field by a quarter-period. Thus, the radiation beam is still in the midplane instead of tilted under the first end pole and thus contributes intense on-axis linearly polarized radiation, which has the effect of diluting the degree of circular polarization from the bulk of the device. This effect is particularly significant at high photon energy because the intensity from other tilted main poles drops sharply due to the shrinking of their vertical distribution width. The end pole configuration shown in Figs. 1a, b can eliminate this end effect (as shown by the dashed curve in Fig. 3).

An intuitively reasonable figure of merit for a circularly-polarized photon source is the product of the circularly polarized intensity F_c and the circular polarization degree P_c . Furthermore, $\sqrt{F_c P_c}$ is proportional to the signal-to-noise ratio in circular dichroism experiments [8]. Fig. 4 shows the distribution of $F_c P_c$ as a function of photon energy and vertical angle. The peak-valley structure tells us which region(s) we should select so as to provide optimized circularly-polarized radiation. The highest peak is located on-axis around half the critical energy. For high photon energies, there are four peaks in the vertical distribution, suggesting that it may be advantageous to use off-axis radiation. However, for high-energy photons, K_x must be decreased to obtain a sufficiently high photon flux; meanwhile, the two central peaks will have merged into one.

The panoramic view of the radiation flux density and polarization degree distributions provide a clear understanding of the general features of circularly-polarized radiation from an elliptical wiggler. In particular, it shows that vertically we should use the on-axis part of the radiation, while horizontally we can collect radiation within a large acceptance angle. It is also clear that the best performance of an elliptical wiggler is for photon energies of the order of E_c . Thus, for very low photon energies, one needs to decrease E_c by reducing the vertical field. In such a case, the horizontal fan width is decreased also. This will impact the layout of beamlines. In contrast to the influence of K_x , changing K_y does not change the distribution patterns other than a scaling of the photon energy axis via E/E_c , e.g. if we double the critical energy, the axis label should be scaled by a factor 2.

4. Some practical considerations in the design of the ALS elliptical wiggler

4.1. End structure and its effects

A commonly-used wiggler-pole excitation pattern places the first several poles on scalar potentials (normalized to that of the poles in the periodic section) $0, 1/2, -1, +1, \dots$, thereby displacing the electron beam in the wiggler from the nominal beam axis by an amount

$$\Delta d = \rho \frac{\pi K}{2} \frac{K}{\gamma k} = \rho \frac{\pi}{2} a,$$

where a is an oscillation amplitude and $\rho \geq 1$, the exact value depending on the harmonic content of the B field [9]. For the proposed elliptical wiggler, assuming $\rho = 1.5$, Δd can be 0.96 mm horizontally and $39 \mu\text{m}$ (for $K_x = 1.5$) vertically. Thus, the source can have about 0.75 mm horizontal shift when we change the vertical gap and $78 \mu\text{m}$ vertical shift when we flip the horizontal field to reverse the photon handedness. Since the photon handed-

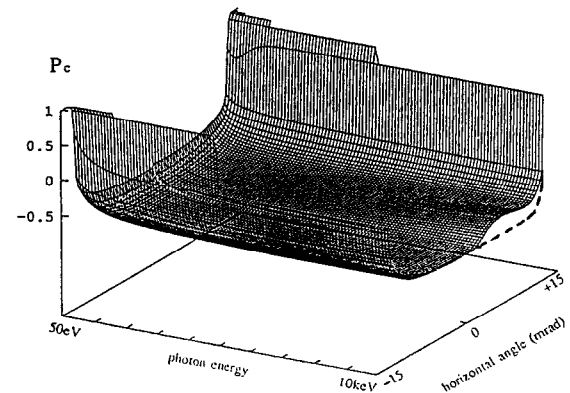


Fig. 3. Photon energy and horizontal angle dependence of circular polarization degree.

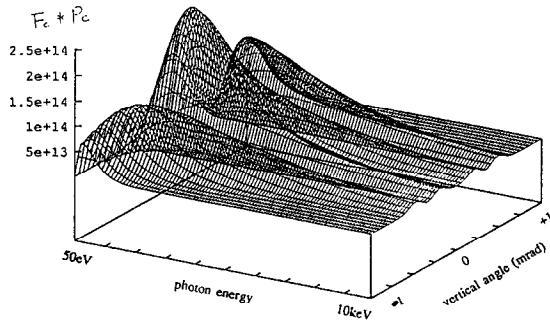


Fig. 4. Figure of merit $F_c P_c$ versus off-midplane position for the energy range 50 eV to 10 keV.

ness is required to oscillate at about 1 Hz [10], the 78 μm vertical beam axis oscillation is of practical concern. To avoid these problems, as shown in Figs. 1a, b the first several poles at the horizontal EM structure's entrance (and exit) are energized such that they lie on scalar potentials 0, +1/4, -3/4, +1, -1, +1, ..., thereby centering the vertical electron spatial oscillations in the periodic section about the nominal beam axis. Thus, the right-versus left-circularly-polarized beamline radiation produced does not shift vertically with the ac oscillations of the electromagnet poles (with perhaps the exception of that produced in the end poles). PM poles in the vertical structure's end sections are likewise energized 0, +1/4, -3/4, +1, -1, +1, ..., so as to maintain the ratio $T_B \equiv B_y(z)/B_x(z \pm \lambda/4)$ constant throughout the end sections.

Even so, the quarter-period axial shift of the vertical vs. horizontal poles implies that one transverse field component ramps up/down one-quarter period before/after the other at the entrance/exit end, contributing linearly-polarized on-axis radiation, thereby reducing the degree of circular polarization, as shown in Fig. 3. This second detrimental effect is minimized in the ALS design where the number of EM wiggler poles, which give rise to the much smaller horizontal field, exceeds that of the number of PM poles by 1, resulting in the EM structure extending $\frac{1}{4}$ period past the PM structure at each end of the wiggler. Furthermore, the first energized pole is just half that of the usual case. Note the 0, +1/4, -3/4, +1 ramp-up at the ends is beam-steering-free and displacement-free independent of whether there are an odd or even number of poles.

A third problem is minimized by choosing an even number of PM poles so that contributions to integrated normal dipole and sextupole from upstream poles at potentials +1/4, -3/4, +1 are canceled by contributions from downstream poles at potentials -1, +3/4, -1/4, respectively. This diminishes the need for storage ring imposed end corrections. Correction of skew dipole and sextupole arising from the differential contributions of the EM poles nominally on potentials +1/4, -3/4, +1, -3/4, +1/4 is likely unnecessary because of the smaller

(by more than a factor of 10) magnitude of the horizontal field and the somewhat larger skew field tolerance specifications. The even number of PM poles makes the upstreammost and downstreammost dipole sources, which are slightly off the midplane, flip together spatially in the vertical direction so these radiation contributions oscillate. However, the effect on on-axis radiation is negligible.

4.2. ALS elliptical wiggler design parameters

Most ALS users are interested in the energy range 500 to 1500 eV, while there has been interest expressed in energies as low as 50 eV and as high as 10 keV. [10] The design parameter $B_y^{\text{max}} = 2$ T is determined by three main factors. First, for the ALS 1.5 GeV ring, significant 10 keV radiation requires a 2 T or even higher magnetic field. Second, 2 T is about the maximum field readily attainable by hybrid-magnet technology. Third, an elliptical wiggler performs best to generate photons of energy around $0.45E_c$ [11], so the 2 T maximum field allows best possible performance up to 1.5 keV. Corresponding to the 2 T peak field, a 20 cm period length and 14 periods are chosen [7]. As described in section 3, the vertical field must be decreased for very low photon energies. The minimum vertical field to be used is determined by radiation optimization considerations [11] and the proposed 5 mrad horizontal acceptance angle [10]. For 0.5 T, the elliptical wiggler can have best performance down to 350 eV; a lower field results in the radiation fan width smaller than the acceptance angle, which reduces the total output from the elliptical wiggler. The best performance range of the ALS elliptical wiggler fits the 500–1500 eV range well. Over this range, within a 5×0.3 mrad² on-axis aperture, 5×10^{14} photons/s/0.1% can be obtained with $P_c \sim 82\%$ and $IP_c^2 \sim 3 \times 10^{14}$. The horizontal field mainly controls the trade-off between degree of circular polarization and flux. Over the best performance range, $K_x \approx 0.9$ is required. According to the maps represented in ref. [11], $K_x = 1.5$ is required to reach 50 eV (even with B_y decreased to 0.5 T) and provide about 80% figure of merit and 85% P_c . The choice of $K_x^{\text{max}} = 1.5$ also depends on the trade-off between performance and cost. The elliptical wiggler performance is flux limited at high energies by B_y^{max} and circular polarization degree limited at low energies by K_x^{max} . For the ALS device, to reach 10 keV the flux drops an order of magnitude with $B_y = 2.0$ T. Note that the values quoted here assume an ideal sinusoidal magnetic field. For the actual designed fields, the harmonics make the magnetic field peaks narrower, resulting in a decrease of the horizontal flux density distribution width from the ideal $\pm K_y/\gamma \sim 12$ mrad, especially for high energy photons. Other radiation properties, such as on-axis spectrum, are substantially unchanged. Electron beam emittance for the ALS will not significantly change the results. The effect of acceptance angle has been treated in a companion paper [11].

Acknowledgments

The authors thank R. Dejus for providing his 3D trajectory calculation code, which is used for the trajectory calculations in this work. This work was supported by the Director, Office of Energy Research, Office of Basic Energy Science, Materials Science Division of the U.S. Department of Energy, under contract No. DE-AC03-76SF00098.

References

- [1] S. Yamamoto, H. Kawata, H. Kitamura, M. Ando, N. Saki and N. Shiotani, *Phys. Rev. Lett.* 62 (1989) 2672.
- [2] C.X. Wang and D. Xian, *Nucl. Instr. and Meth. A* 288 (1990) 649.
- [3] C.X. Wang, *SPIE Proc.* 2013 (1993) 126.
- [4] C.X. Wang and Y. Xiao, in: *Proc. Int. Conf. on Synchrotron Radiation Sources*, Indore, India, 1992, eds. S.S. Ramamurthi, G. Singh, and D. Angal.
- [5] F.W.J. Olver, *Asymptotics and Special Functions* (Academic Press, New York, 1974).
- [6] M. Born and E. Wolf, *Principles of Optics*, 6th ed. (Pergamon Press Inc, New York, 1980) p. 317.
- [7] E. Hoyer, LSME M7281A, LBL, 1993.
- [8] C. Bustamante, C.T. Chen, F. Sette, M.R. Howells, A.J. Hunt, K.J. Kim, B.M. Kincaid, M.F. Maestre, D.R. Nygren, M. Wons, P.A. Snyder and E.A. Stern, *Rev. Sci. Instr.* 63 (1992) 1346.
- [9] K. Halbach, *Nucl. Instr. and Meth. A* 250 (1986) 95.
- [10] Working Group on Elliptical Wiggler (April, 1993), LBL-33996.
- [11] C.X. Wang and R. Schlueter, these Proceedings (8th Nat. Conf. on Synchrotron Radiation Instrumentation, Gaithersburg, MD, USA, 1993) *Nucl. Instr. and Meth. A* 347 (1994) 92.